Journal of Electronic Materials (2023) 52:5822–5833
https://doi.org/10.1007/s11664-023-10527-2

ORIGINAL RESEARCH ARTICLE

P3HT-Based Semi-Conductive Electrospun Nanocomposite Fibrous Emitters Doped with $CsPbBr_3$ Perovskite Quantum Dots

Georgia Papaparaskeva[1] · Maria Lydia Ioannides[1] · Chryso Lambride[1] · Eugenia Tanasă[2] · Theodora Krasia-Christoforou[1]

Received: 17 January 2023 / Accepted: 22 May 2023 / Published online: 20 June 2023

Abstract

Poly(3-hexylthiophene-2,5-diyl) (P3HT)-based semiconducting electrospun nanocomposite fibrous emitters were successfully fabricated by combining P3HT with poly(ethylene oxide) (PEO) and commercially available $CsPbBr_3$ perovskite quantum dots (PQDs). The latter were employed as a synergistic photoluminescence emitter of high efficiency within the P3HT/PEO blended polymer matrix, while PEO was used as an auxiliary polymer to assist the electrospinnability of P3HT. The produced materials were characterized with respect to their chemical composition and morphology by scanning electron microscopy (SEM) and transmission electron microscopy/energy-dispersive x-ray analysis (TEM/EDX) whereas fluorescence microscopy and spectroscopy were employed to study their optical properties. Based on the obtained results, it was confirmed that the PQDs were successfully encapsulated within the electrospun fibers at a high percentage (10 wt.%), retaining at the same time their optical properties and nanoscale dimensions. Moreover, the experimental data obtained suggested the existence of inter-material interactions between P3HT and PQDs. Consequently, this study creates new pathways in the development of innovative fibrous nanocomposites with unique optoelectronic features, rendering them highly interesting in light-harvesting, sensing and optoelectronic applications.

Graphic Abstract

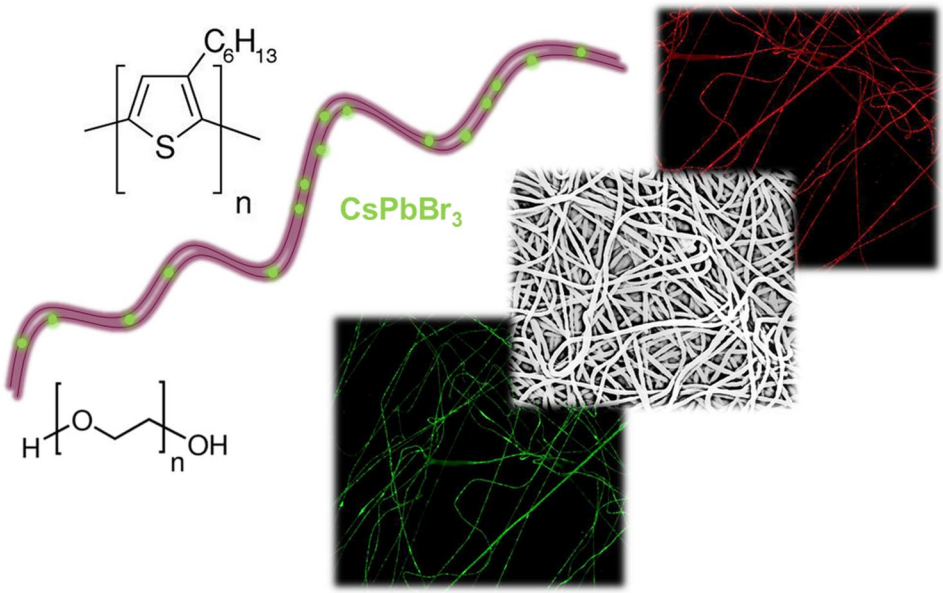

Maria Lydia Ioannides and Chryso Lambride have contributed equally to this work.

Extended author information available on the last page of the article

Keywords Electrospinning · $CsPbBr_3$ perovskites · perovskite quantum dots (PQDs) · poly(3-hexylthiophene-2,5-diyl) (P3HT) · poly(ethylene oxide) (PEO) · conductive fibers · fibrous emitters

Introduction

Over the last decade, colloidal lead halide perovskite (LHP) nanocrystals (NCs), denoted as $APbX_3$ [X = Cl, Br, I], of either hybrid organic–inorganic [A = FA, $CH_3(NH_2)_2^+$ or A = MA, $CH_3NH_3^+$] or all-inorganic [A = Cs] chemical composition, have attracted enormous interest in the field of advanced optoelectronic materials. These semiconducting NCs have been highlighted as highly efficient photoluminescent (PL) materials due to their tunable energy band gaps across the visible light spectrum region, with narrow line widths and high emission quantum yields (QYs). Different cost-effective synthetic methodologies have been employed for the preparation of such materials, allowing for the fine-tuning of their chemical composition.[1–4]

LHP NC emitters exhibit notable optoelectronic features including large absorption coefficients, high charge carrier mobility and long exciton diffusion lengths,[5] thus rendering them very promising in various photonic and electronic applications such as solar cells, light-emitting diodes (LEDs), transistors and photodetectors.[6–12]

Electrospinning is considered to be one of the most versatile electrohydrodynamic processes that is widely used in the fabrication of nano- and microfibers of various chemical compositions and morphologies. Because of its simplicity, cost-effectiveness and scalability,[13,14] this technique is used worldwide in the production of multifunctional nano- and microfibrous materials with potential use in optoelectronics, catalysis, sensing, energy, and biomedicine.[15–18] Moreover, electrospinning allows the incorporation of nanomaterials including nanoparticles, nanowires, nanotubes and nanoplatelets[19] within the produced (nano)fibers, retaining at the same time their intrinsic structural characteristics and physicochemical properties.

In the field of photonics, organic–inorganic semiconductor fibrous nanocomposites produced by electrospinning have recently attracted considerable attention.[20] More precisely, researchers aim to fabricate flexible optoelectronic materials by integrating LHP NCs within electrospun polymer fibers.[21] Examples include the incorporation of methylammonium lead triiodide perovskites ($CH_3NH_3PbI_3$, $MAPbI_3$) within polyacrylonitrile (PAN) and polyvinylpyrrolidone (PVP) electrospun fibers[22,23] as well as the fabrication of polystyrene (PS) and polymer vinyl acetate (PVAc) electrospun fibers loaded with $CsPbX_3$ (X = Br, I, and Cl) nanocrystals and aligned $CsPbBr_3$ nanorods generated in situ.[24,25] In another example, 3D multi-layered assemblies consisting of electrospun poly(vinylidene fluoride) (PVDF) nanofibers and electrosprayed $CsPbBr_3$@PVDF particles were developed and evaluated as high-performance flexible piezoelectric nanogenerators.[26]

Recently, our group reported the fabrication of robust and bright polymer electrospun fibrous emitters, based on either the hydrophilic PVP or the hydrophobic poly(methyl methacrylate) (PMMA), sensitized by green-emitting all-inorganic $CsPbBr_3$ or hybrid organic–inorganic $FAPbBr_3$ nanocrystals.[27] One of the main limitations of LHP NC emitters is their high sensitivity and consequently low compositional stability resulting from thermodynamic spontaneous activation of structural degradation mechanisms, especially when these are exposed to ambient conditions.[28–30] In our study it was demonstrated that the encapsulation of the NCs within electrospun fibers enhances their optical stability over an extended exposure in air or upon immersion in water compared to the pristine NC films.

While in the few existing examples dealing with the fabrication of polymer-based electrospun fibrous nanocomposite emitters with embedded perovskite NCs, such materials appear particularly attractive in optoelectronic applications,[31–35] to the best of our knowledge, in none of these examples NCs have been combined with conductive polymers. In contrast, several studies have described the generation of nanocomposites in a film form, based on conductive polymers including poly(3-hexylthiophene) (P3HT), polypyrrole (PPy) and poly(aniline) (PANI) and perovskites.[36–39]

In the present study, the fabrication and characterization in terms of morphology, chemical composition and fluorescence properties of electrospun fibrous nanocomposites consisting of poly(3-hexylthiophene) (P3HT)-based electrospun nanofibers and photoluminescent $CsPbBr_3$ quantum dots (QDs) is presented and discussed. This work creates new prospects towards the development of novel optoelectronic materials based on electrospun conductive nanofibers and perovskite NC emitters with tunable fluorescence properties, since it is demonstrated that the fibers' spectral emission profile can be enhanced by increasing the perovskite content up to 10 wt.% Specifically, by encapsulating highly stable $CsPbBr_{3)}$ perovskite quantum dots (PQDs) within P3HT/poly(ethylene oxide) (PEO) electrospun fibers, a significant enhancement in the fluorescence intensity of the electrospun fibers was observed (i.e. 45% enhancement) in the presence of 10 wt.% $CsPbBr_3$ QDs. Hence, the present study paves the way for the fabrication of nanocomposite photoconductive

(nano)fabrics that can be used as lightweight materials in applications such as organic optoelectronic memory devices, photosensors and solar cells.

Experimental Part

Materials

Poly(3-hexylthiophene-2,5-diyl) (P3HT) (MW = 50–70 KDa, polydispersity: 1.4–1.6, RR = 93–95%) was purchased from Solaris Chem Inc. Poly(ethylene oxide) (PEO) (MW = 600,000 g mol^{-1}) was obtained from Sigma-Aldrich. Both polymers were used without further purification. Chloroform ($CHCl_3$, analytical grade, Scharlau Chemicals) was the solvent employed in the preparation of the P3HT/PEO fibers and P3HT/PEO/$CsPbBr_3$ electrospun fibrous emitters as described in the next section. $CsPbBr_3$ PQDs stabilized in toluene, coated with oleic acid and oleylamine (solution concentration: 10 mg/mL; emission wavelength 505–515 nm; appearance/color: green to yellow), were purchased from Sigma-Aldrich and used as received by the supplier.

Preparation of P3HT/PEO and P3HT/PEO/$CsPbBr_3$ Solutions

For the fabrication of neat P3HT/PEO electrospun fibers, a P3HT (20 wt.%)/PEO (80 wt.%) blended polymer solution was prepared as follows. P3HT (0.0168 g) and PEO (0.0672 g) were separately dissolved in $CHCl_3$ (1.0 mL at 300 rpm and 1.3 mL at 600 rpm, respectively). The two solutions were left under stirring for 24 h at room temperature until complete dissolution. Subsequently, an additional amount of $CHCl_3$ (0.5 mL) was added to the P3HT-$CHCl_3$ solution, which was then mixed with the PEO-$CHCl_3$ solution. The resulting mixture was left under stirring (300 rpm) for 48 h at room temperature. The final highly homogeneous solution (final solution concentration: 3% w/v) was used in the fabrication of blended P3HT/PEO fibers by electrospinning.

For the preparation of P3HT/PEO/$CsPbBr_3$ solutions, two different PQD loading percentages were employed (5 wt.%, and 10 wt.% with respect to the total polymer mass). Initially, the aforementioned synthetic procedure followed for the preparation of the P3HT/PEO blended polymer solution was likewise repeated. After 72 h of stirring under ambient conditions, the proper volume of the PQD solution was added to the blended polymer solution (i.e., for 5 wt.%: 442.1 µl (4.421 mg) and for 10 wt.%: 884.2 µl (8.842 mg)), followed by 1 min of mixing using a Vortex mixer (MRC Laboratory Instruments).

Fabrication of Electrospun P3HT/PEO Fibers and Nanocomposite P3HT/PEO/$CsPbBr_3$ Fibrous Emitters

P3HT/PEO with a 20/80 wt.%, denoted as P3HT/PEO, P3HT/PEO with a 5 wt.% $CsPbBr_3$ in respect to the total polymer mass (denoted as P3HT/PEO/$CsPbBr_3$ (5 wt.%)) and P3HT/PEO with a 10 wt.% $CsPbBr_3$ in respect to the total polymer mass (denoted as P3HT/PEO/$CsPbBr_3$ (10 wt.%)) solutions prepared as described in the previous section were loaded into a 10 mL glass syringe to be further electrospun. All electrospinning experiments were performed at room temperature. The electrospinning set-up included a controlled-flow, four-channel volumetric microdialysis pump (KD Scientific, model: 789252), 10 mL glass syringe with metallic needle (25 G) and with specially connected spinneret needle electrodes, a high-voltage power generator (10–50 kV, ES50P-20W Gamma High Voltage Research) and a custom-designed grounded target collector (282 mm length × 279 mm height), inside an interlocked Faraday enclosure safety cabinet.

Systematic parametric studies were performed, and the optimum electrospinning conditions for obtaining continuous, bead-free fibers characterized by high homogeneity in terms of diameter, corresponding to (a) P3HT/PEO, (b) P3HT/PEO/$CsPbBr_3$ (5 wt.%) and (c) P3HT/PEO/$CsPbBr_3$ (10 wt.%) were obtained as follows: applied voltage: (a) 15 kV, (b) 16.5 kV and (c) 20.5 kV; flow rate: (a)–(c) 2.5 mL/h; needle-to-collector distance: (a)–(c) 15 cm; and needle gauge: (a)–(c) 25 G.

Material Characterization

Scanning Electron Microscopy (SEM)

The morphology and diameter of the P3HT/PEO and P3HT/PEO/$CsPbBr_3$ fibrous membranes were determined by scanning electron Microscopy (SEM) (Vega TS5136LS-Tescan). The samples were gold-sputtered (~15 nm) (sputtering system K575X Turbo Sputter Coater, Emitech) prior to SEM inspection. The average fiber diameters and their distribution were measured using image analysis software (ImageJ) by measuring at least 15 fibers in SEM images.

Transmission Electron Microscopy (TEM)

Transmission Electron Microscopy (TEM) was performed by using a TECNAI F30 G2 S-TWIN microscope operating at 300 kV equipped with an energy dispersive x-ray spectrometer (EDX). Samples were placed into a double copper grid (oyster) to be visualized by TEM. The average size

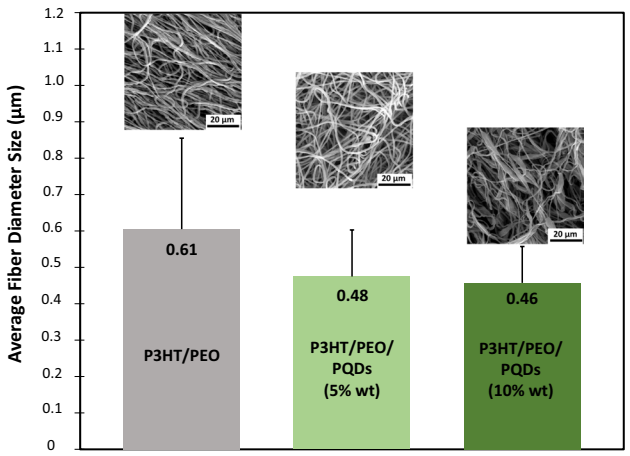

Fig. 1 SEM images of P3HT/PEO (left image); P3HT/PEO/$CsPbBr_3$ (5 wt.%) (middle image); and P3HT /PEO/$CsPbBr_3$ (10 wt.%) (right image). Average fiber diameter analysis + standard deviation (SD) of the produced fibrous analogues, calculated using ImageJ corresponding to P3HT/PEO: 0.61 ± 0.25 (μm); P3HT/PEO/$CsPbBr_3$ (5%): 0.48 ± 0.13 (μm); and P3HT /PEO/$CsPbBr_3$ (10%): 0.46 ± 0.17 (μm). Sampling size: 15 fibers.

of the $CsPbBr_3$ PQDs embedded within the P3HT/PEO/$CsPbBr_3$ fibrous membranes were determined using ImageJ software, considering at least 30 PQDs in TEM images.

X-ray Diffraction Analysis

XRD patterns were recorded by using powder x-ray diffraction (PXRD) in a Rigaku SmartLab diffractometer (CuKα radiation; $\lambda = 0.154$ nm) with a scanning rate of 1°/min over the 2θ range of 3°–50°. For the XRD analysis, the P3HT/PEO and P3HT/PEO/$CsPbBr_3$ fibrous mats were deposited on a quartz-coated glass slide.

Mechanical Testing

Tensile experiments were performed using a high-precision mechanical testing system (Instron 5944, Norwood, MA, USA). The specimens were cut in an orthogonal shape with dimensions 5 × 4 × 0.5 mm (length × width × thickness) and placed between two parallel grips. Stress–strain experiments were performed to test the elastic response of the material. The specimens were stretched to 25% strain with a strain rate of 0.5 mm/min. The stress was calculated as the force measured on the load cell divided by the initial area of the specimen and the strain was calculated as the displacement Δl divided by the initial length of the specimen. The Young's modulus was calculated from the slope of the linear part of the stress–strain curves for low strains (< 5%). Three specimens for each case were tested.

Fluorescence Microscopy and Spectroscopy

The P3HT/PEO and nanocomposite P3HT/PEO/$CsPbBr_3$ fibrous emitters were analyzed by fluorescence microscopy. The samples were placed on glass slides, covered with coverslips and examined using a fluorescence microscope (U-RLF-T model; OLYMPUS XM10 camera). An FITC filter (excitation wavelength: 490 nm; emission wavelength: 525 nm) was employed in the analysis of the perovskite-loaded fibrous emitters as well as in the visualization of the pristine P3HT/PEO fibrous analogues. The obtained images were analyzed by the CellSens Standard and ImageJ software. Images were taken at 20 × magnification.

The fluorescence emission spectra of the pristine P3HT/PEO fibers and the nanocomposite P3HT/PEO/$CsPbBr_3$ analogues were recorded by using a Jasco FP-6300 fluorescence spectrophotometer (Jasco Incorporated, Easton, MD, USA). The excitation and emission wavelength were set at 450 nm and 560 nm, respectively and a 480 nm high band-pass filter was placed between the sample cuvette and the detector, so as to avoid higher order emitted light effects.

Results and Discussion

Fabrication and Morphological Characterization of Electrospun P3HT/PEO, P3HT/PEO/$CsPbBr_3$ Fibrous Emitters

P3HT is a semi-crystalline, hydrophobic and highly conductive polymer that has been widely used as an extremely efficient hole-transport material (HTM) in perovskite $MAPbI_3$-based solar cells (PCs) in the film form.[40] Very recently, efficiency improvement for lead-free perovskite-inspired $Cs_3Sb_2I_9$ solar cells introducing P3HT as the hole transport material has been reported.[41] P3HT was further explored in various optoelectronic applications including rechargeable battery electrodes,[42] electrochromic devices,[43] optical and chemical sensors,[44–46] light-emitting diodes,[47] field-effect transistors[48] and non-linear optical materials.[49]

The rigid backbone of P3HT makes it impossible to be processed by electrospinning, since the required level of chain entanglements enabling the formation of fibers is not favored.[50] To overcome this limitation, the use of polyethylene oxide (PEO) as the electrospinnable secondary component has been proposed, enabling the successful production of blended P3HT/PEO electrospun fibers.[51,52]

We have recently reported the fabrication and characterization of highly aligned electrospun P3HT-rich electrospun fibrous systems (i.e., P3HT/PEO wt.%, 80:20; P3HT/PEO wt.%, 95:5) using a corrugated static collector.[53] Based on our previous knowledge regarding the

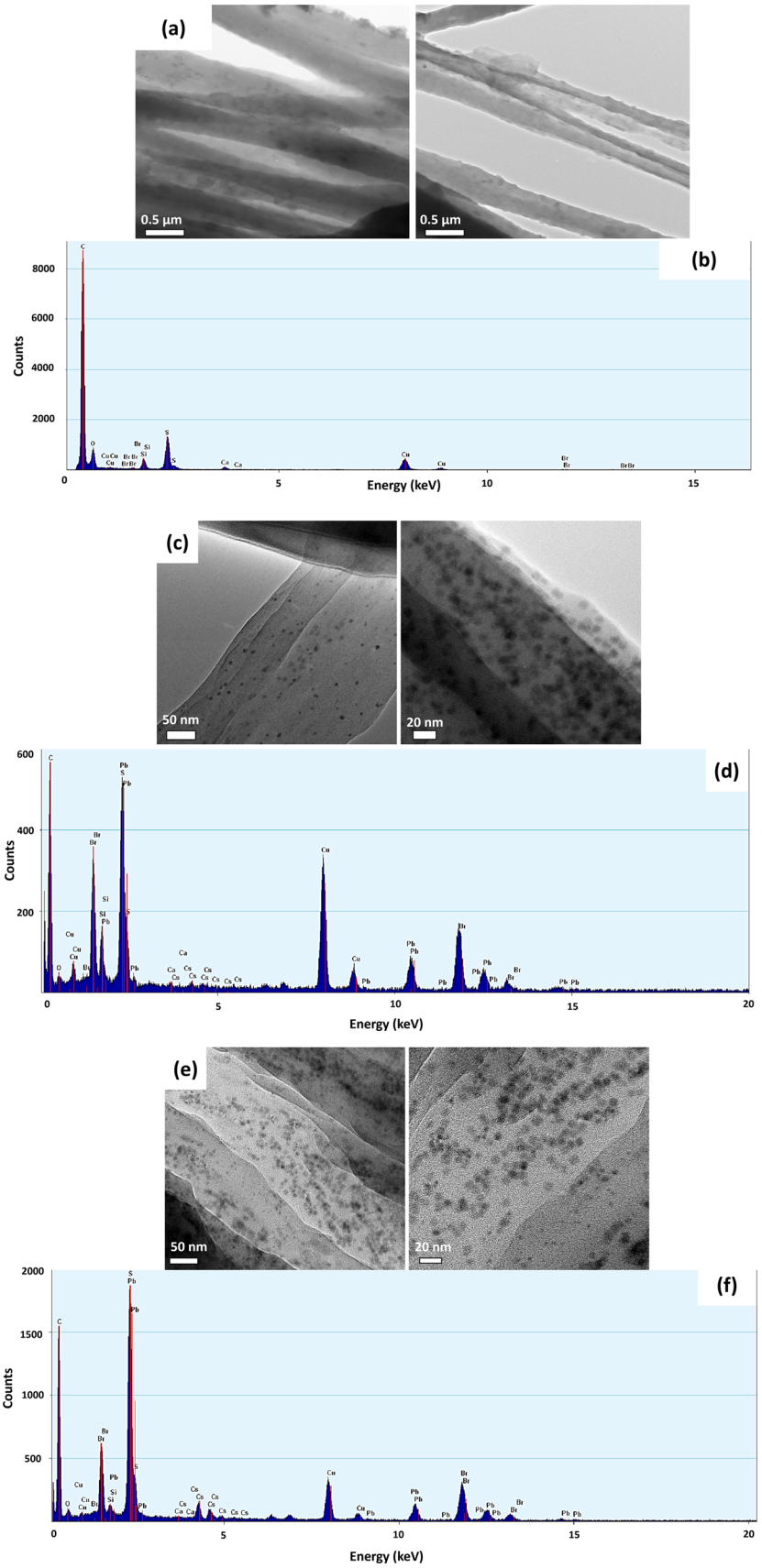

Fig. 2 TEM bright field images and corresponding EDX spectra of the P3HT/PEO electrospun fibers (a), (b), P3HT/PEO/$CsPbBr_3$ (5 wt.%) (c), (d), and P3HT/PEO/$CsPbBr_3$ (10 wt.%) (e), (f) nanocomposite fibers.

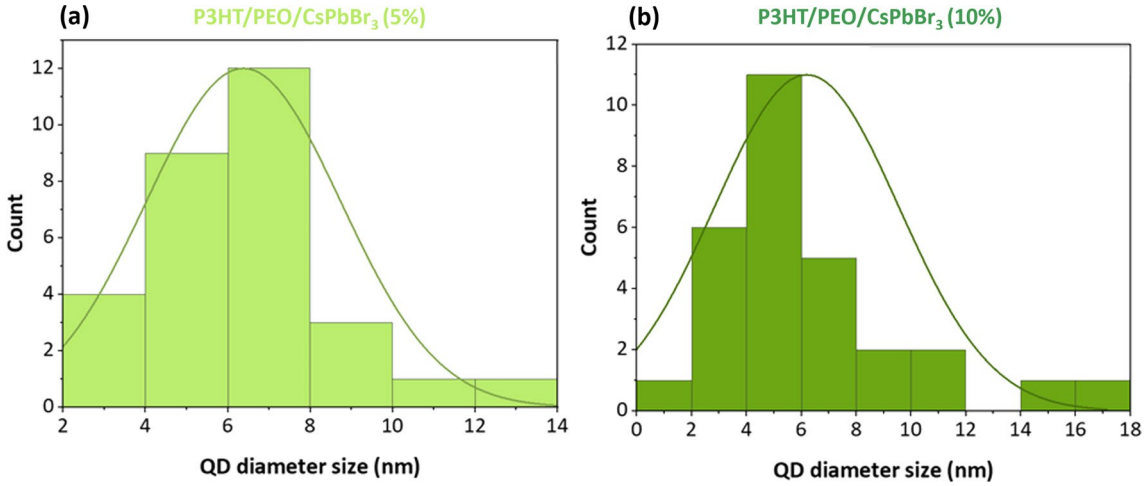

Fig. 3 PQD diameter size and size distribution. (a) P3HT/PEO/$CsPbBr_3$ nanocomposite fibers with 5 wt.% perovskite PQD loading: average PQD diameter analysis + standard deviation (SD) after electrospinning: 6.4 ± 2.4 (nm) and (b) P3HT/PEO/$CsPbBr_3$ nanocomposite fibers with 10 wt.% PQD loading: average PQD diameter analysis + standard deviation (SD) after electrospinning: 6.16 ± 3.3 (nm). Number of counts: 30.

Table I Main experimental findings deriving from the TEM/EDS analysis of the pristine and the PQD-loaded P3HT/PEO electrospun fibers with variable (5 wt.% and 10 wt.%) PQD content

System	Average PQD diameter + SD (nm)	Elements present
P3HT/PEO	–	C, O, S and Cu (from grid)
P3HT/PEO/$CsPbBr_3$ (5 wt.%)	6.4 ± 2.4	Pb, Br, Cs, C, O, S and Cu (from grid)
P3HT/PEO/$CsPbBr_3$ (10 wt.%)	6.16 ± 3.3	Pb, Br, Cs, C, O, S and Cu (from grid)

experimental parameters for processing P3HT/PEO polymer solutions, in this study, the optimum electrospinning conditions were facilely defined, resulting in P3HT/PEO and P3HT/PEO/$CsPbBr_3$ electrospun fibrous mats (see supplementary Figure S1).

The morphological characteristics of the produced fibers were investigated by SEM. As seen in Fig. 1, continuous, uniform fibers having consistent fiber diameters could be obtained in all cases. Even though the PQD content is exceptionally high compared to previous studies on perovskite NC-loaded electrospun fibers, [27,54–58] no PQD aggregates can be observed on the fiber surfaces (Fig. 1, middle and right images), which indicates their successful incorporation and homogeneous distribution within the P3HT/PEO fibers, while retaining their nanoscale dimensions. However, in the case of the highest PQD loading (10 wt.%), the homogeneous cylindrical fiber morphology is disrupted as seen in Fig. 1 (right image).

From the analysis of the SEM images, the average fiber diameters were calculated to be 0.61 ± 0.25 μm, 0.48 ± 0.13 μm and 0.46 ± 0.17 μm for the pristine P3HT/PEO nanofibers and the corresponding systems containing 5 wt.% and 10 wt.% $CsPbBr_3$ QDs, respectively. The pristine (P3HT/PEO) and nanocomposite (P3HT/PEO/$CsPbBr_3$) fibers were further characterized by TEM/EDX. Figure 2 provides characteristic TEM images and corresponding EDX spectra of the aforementioned materials. In the case of the pristine P3HT/PEO fibers, TEM revealed their textured surface morphology (Fig. 2a), which is likely attributed to the existing immiscibility between P3HT and PEO, resulting in phase separation phenomena. The corresponding EDX spectrum (Fig. 2b) shows the presence of C, O and S as the major elements in the sample (Cu comes from the copper grid). The presence of minor elements (Si, Br, Ca) is attributed to mild sample contamination during the preparation process for TEM investigations. The existence of the $CsPbBr_3$ QDs within the P3HT/PEO electrospun fibers can be clearly observed at different QD loading percentages as seen in the TEM images provided in Fig. 2c, d, e and f, corresponding to the P3HT/PEO/$CsPbBr_3$ nanocomposite fibrous emitters with 5 wt.% and 10 wt.% PQD content, respectively. By

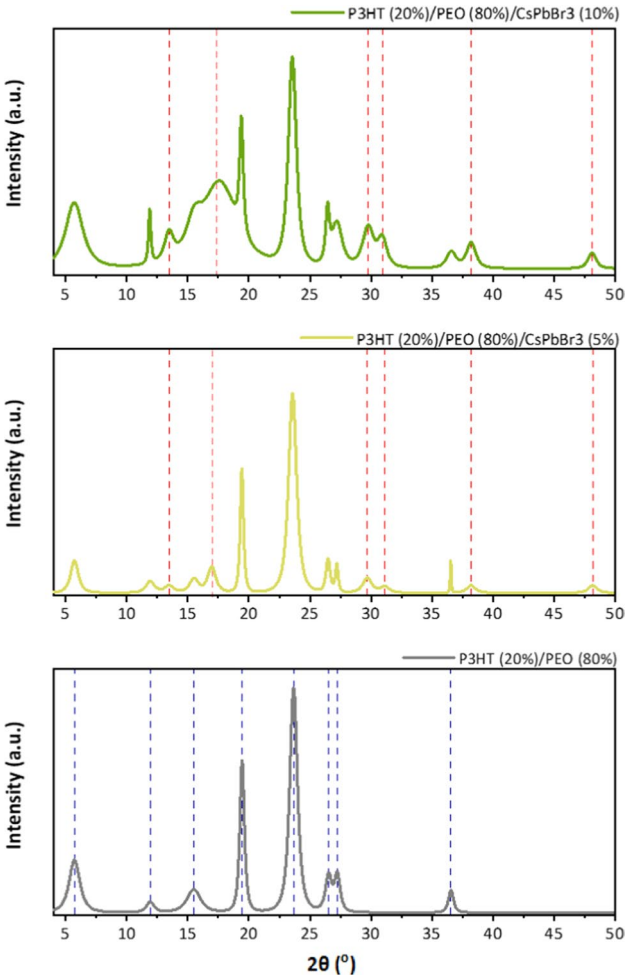

Fig. 4 XRD spectra corresponding to the pristine (P3HT/PEO) and the nanocomposite (P3HT/PEO/$CsPbBr_3$ (5 wt.%); P3HT/PEO/$CsPbBr_3$ (10 wt.%)) systems. Blue dotted lines denote characteristic XRD signals of P3HT and PEO. Red dotted lines correspond to characteristic XRD signals of the PQDs embedded within the polymer matrix (data provided with background correction) (Color figure online).

comparing the morphology and dimensions of the perovskite QDs embedded within the fibers with those of the as-purchased QDs (i.e., < 10 nm) it can be concluded that no severe agglomeration phenomena occurred during the electrospinning process since their small dimensions and spherical morphology are both retained (Fig. 3a and b). The corresponding EDX spectra appearing in Fig. 2d (P3HT/PEO/$CsPbBr_3$ (5 wt.%)) and 2f (P3HT/PEO/$CsPbBr_3$ (10 wt.%)), show the presence of Pb, Br and Cs (in addition to C, O, and S) as major elements in the sample, attributed to the existence of $CsPbBr_3$ PQDs within the polymer matrix. Table I summarizes the main information derived from the TEM/EDS analysis of the three systems.

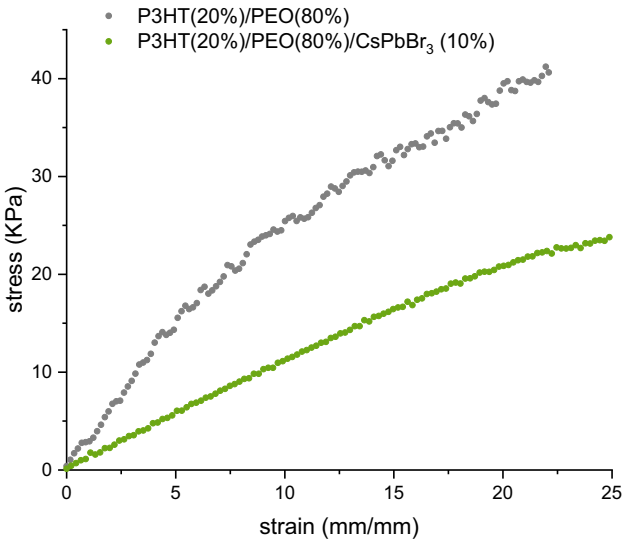

Fig. 5 Stress–strain curves recorded under tensile conditions for the P3HT/PEO fibrous membrane (grey) and the PQD-functionalized electrospun nanocomposite membrane (green) (Color figure online).

X-ray Diffraction Analysis

XRD was employed to obtain information on the crystalline structure and chemical composition of the produced materials. Because of the semi-crystalline nature of P3HT and PEO, characteristic diffraction signals appear in the XRD spectrum of the neat P3HT/PEO fibers, provided in Fig. 4. Typically, P3HT presents well-defined peaks at 2θ between 20° and 25° and PEO at around 19°–23°. In our study, characteristic XRD peaks appearing at 2θ values of 5.72°, 19.44°, and 23.66° correspond to the diffraction peaks from (100) planes of P3HT, (120) planes of PEO, and (010) planes of P3HT, respectively.

The XRD pattern of $CsPbBr_3$ typically exhibits a series of well-defined peaks at 2θ values between 10 and 40°. Thus, the most prominent characteristic peaks appearing in the XRD spectra of $CsPbBr_3$-based P3HT/PEO fibers at 2θ values of 13.45° (100), 17.27° (110), 29.75° (200), 31.00° (210), 38.20° (211), and 48.10°(220) are related to the crystal structure and the chemical composition of PQDs. The corresponding Miller indices for the most prominent XRD peaks of $CsPbBr_3$ PQDs are the (100), (110), (200), (210), (211), and (220) crystal planes. However, in the case of the polymer-PQD composites, the specific position and intensity of the PQDs may depend on various factors, including the crystallinity, morphology and composition of the individual

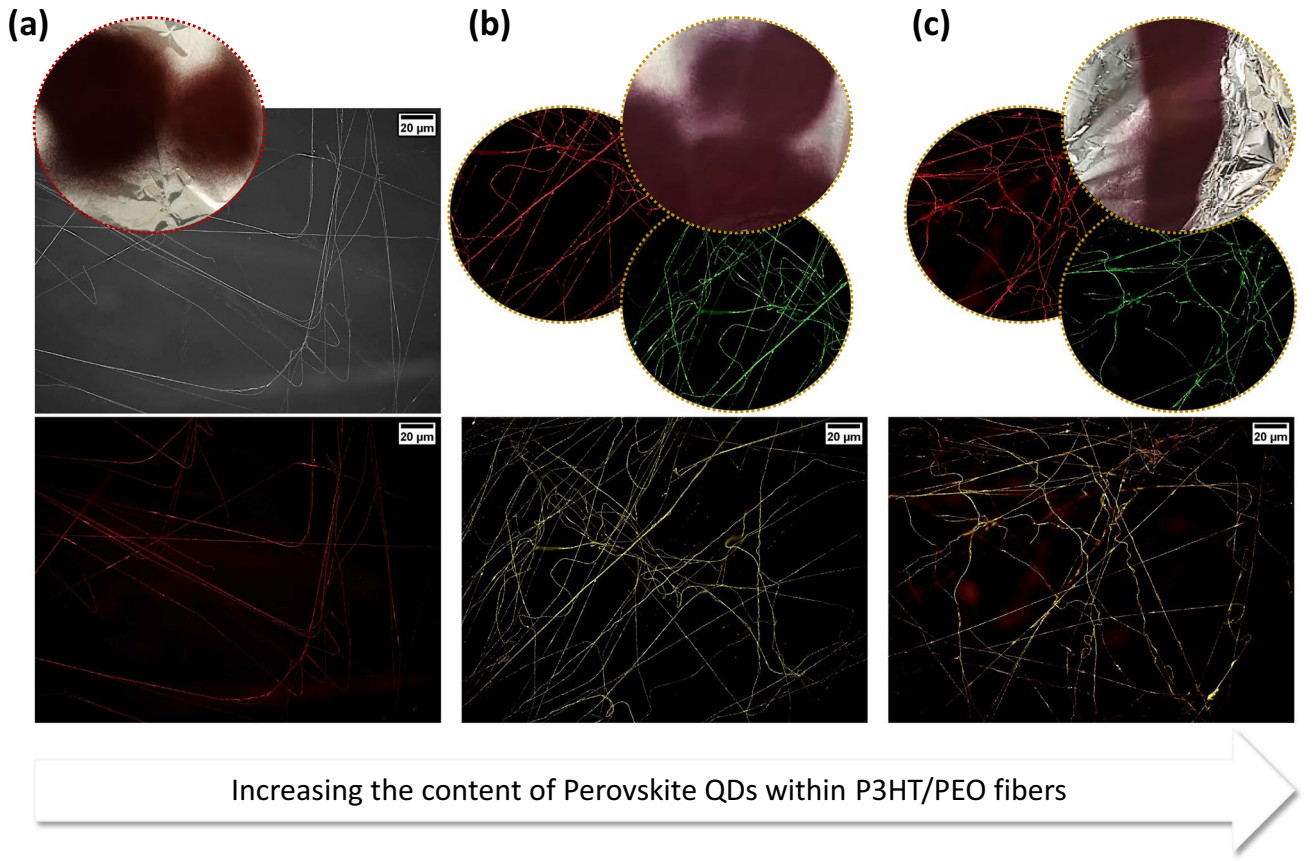

Fig. 6 Photographs and characteristic fluorescence microscopy images of (a) P3HT/PEO; (b) P3HT/PEO/$CsPbBr_3$ (5 wt.%) and (c) P3HT/PEO/$CsPbBr_3$ (10 wt.%) electrospun fibrous membranes.

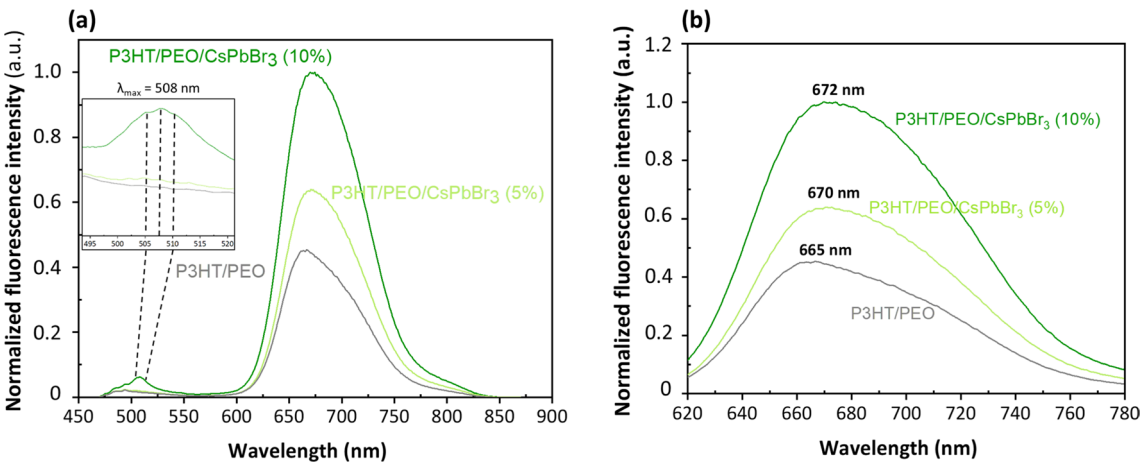

Fig. 7 (a) Comparative optical spectra of the nanocomposite P3HT/PEO/$CsPbBr_3$ fibers with variable PQD content. The inset displays a magnification in the $CsPbBr_3$ PQD emission region. (b) Comparative optical spectra of the nanocomposite P3HT/PEO/$CsPbBr_3$ fibers with variable PQD content in the P3HT emission region.

components, as well as on possible polymer-PQD interactions existing within the composite.

Mechanical Performance

The mechanical properties of the P3HT/PEO (PQD-free) and the P3HT/PEO/$CsPbBr_3$ (10 wt.%, highest PQD loading) electrospun nanocomposite fibrous membranes was investigated under tensile loading conditions. Representative stress–strain curves for each case are provided in Fig. 5. The Young's modulus for each membrane was calculated from the slope of the linear part of the stress–strain curves for low strains (< 5%). The corresponding average values were 11.29 ± 2.18 kPa for pristine and 5.14 ± 1.12 kPa for PQD-functionalized fibrous membranes. This decrease in the material's stiffness observed in the presence of the PQD nanoadditives might be attributed to a decrease in the degree of crystallinity of the PEO and P3HT semi-crystalline polymers in the presence of the PQD nanofillers. More precisely, the degree of crystallinity of semi-crystalline polymers might be significantly influenced in the presence of inorganic nanoparticulates, depending on their size, morphology, loading percentage, dispersion mode and the polymer-nanoparticle interactions.[59]

Optical Properties of the Pristine P3HT/PEO and the Nanocomposite P3HT/PEO/$CsPbBr_3$ Fibers

The optical properties of the pristine polymer fibers (P3HT/PEO) and the corresponding perovskite-sensitized nanocomposite analogues were initially investigated by fluorescence microscopy. Fluorescence microscopy images provided in Fig. 6 reveal the uniformity of the produced fibers, whereas the majority of the embedded PQDs are enfolded within the fibers in a homogeneous manner (in line with the TEM analysis data).

The optical properties of the produced materials were further investigated by fluorescence spectroscopy. The fluorescence spectra of the nanocomposite P3HT/PEO/$CsPbBr_3$ QDs systems with variable QD content are displayed in Fig. 7.

As seen, the spectrum corresponding to the pristine P3HT/PEO fibers presents one dominant peak in the red region (at 665 nm) attributed to the P3HT polymer emission. This result matches the emission peak appearing at 667 nm for previously reported systems based on poly(3-hexylthiophene)/poly(methyl methacrylate) core–shell electrospun fibers developed for sensing applications.[60] Furthermore, the presence of an additional emission peak at 508 nm (green region) in the case of the P3HT/PEO/$CsPbBr_3$ (10 wt.%) system, demonstrates the successful incorporation of PQD within the fibers (Fig. 7a). The corresponding peak appearing in the green region attributed to the P3HT/PEO/$CsPbBr_3$ (5 wt.%) nanocomposite system is significantly weaker, deriving from the lower content of PQDs. Additionally, the maximum P3HT emission signal of the nanocomposite fibers with 5 wt.% and 10 wt.% $CsPbBr_3$ PQDs appears at 670 nm and 672 nm, respectively, in contrast to that corresponding to pure P3HT/PEO fibers that can be seen at 665 nm. Both emission shifts relate to electronic transitions due to the presence of $CsPbBr_3$ PQDs (i.e., redshift observation) (Fig. 7b). Moreover, the encapsulation of $CsPbBr_3$ PQDs significantly influences the fluorescence intensity of the peak corresponding to P3HT emission, exhibiting up to ~ 45% enhancement. This result strongly indicates the existence of inter-material interactions between $CsPbBr_3$ PQDs and P3HT.

Consequently, the present study paves the way towards the design of electrospun perovskite-sensitized conductive fibrous nanocomposites in which the recombination of photogenerated charge carriers can be prevented,[61] thus leading to an improved quantum efficiency, rendering them highly promising in photovoltaic and optoelectronic applications.

Conclusions

In this study blended P3HT/PEO electrospun fibers were successfully combined with $CsPbBr_3$ perovskite quantum dots (PQDs) to yield semiconducting nanocomposite fibrous emitters. SEM analysis verified the generation of homogeneous, bead-free fibers with fiber diameters in the submicrometer scale range, while TEM/EDX revealed the successful incorporation of the perovskite QDs within the P3HT/PEO fibers during the electrospinning process, without observing any severe agglomeration phenomena, even at high PQD loadings. The optical properties of the produced systems were determined by means of fluorescence microscopy and fluorescence spectroscopy. Both techniques showed that the optical properties of both the P3HT and the PQDs were retained within the fibrous nanocomposite structures. Most importantly, the experimental data obtained suggested the existence of inter-material interactions between $CsPbBr_3$ PQDs and P3HT, since a redshift and a significant enhancement in the intensity of the P3HT fluorescence emission signal (up to 45%) were observed. Consequently, the fabrication of nanocomposite fibrous mats in which electro-conductive polymers co-exist with perovskite nanoemitters creates new perspectives in the development of highly efficient nanofibrous emitters

with potential optoelectronic, sensing and light-harvesting applications.

Supplementary Information The online version contains supplementary material available at https://doi.org/10.1007/s11664-023-10527-2.

Acknowledgments We thank the University of Cyprus for financial support and the Cyprus State Scholarship Foundation for supporting with a full scholarship the PhD studies of Ms. Georgia Papaparaskeva. We are grateful to Prof. Epaminondas Leontides (University of Cyprus, Department of Chemistry) for providing access to the fluorescence spectrometer and for the assistance with the corresponding measurements, Dr. Georgios Mesaritis (Department of Mechanical and Manufacturing Engineering, University of Cyprus) for the assistance with the XRD measurements, and Ms. Christina Michael and Dr. Fotios Mpekris (Cancer Biophysics Laboratory, Department of Mechanical and Manufacturing Engineering, University of Cyprus) for the fluorescence microscopy analysis and the performance of the mechanical testing respectively.

Conflict of interest The authors declare that they have no conflict of interest or competing interests.

References

1. L. Protesescu, S. Yakunin, M.I. Bodnarchuk, F. Krieg, R. Caputo, C.H. Hendon, R.X. Yang, A. Walsh, and M.V. Kovalenko, Nanocrystals of cesium lead halide perovskites ($CsPbX_3$, X = Cl, Br, and I): novel optoelectronic materials showing bright emission with wide color gamut. *Nano Lett.* 15, 3692 (2015).
2. L. Protesescu, S. Yakunin, M.I. Bodnarchuk, F. Bertolotti, N. Masciocchi, A. Guagliardi, and M.V. Kovalenko, Monodisperse formamidinium lead bromide nanocrystals with bright and stable green photoluminescence. *J. Am. Chem. Soc.* 138, 14202 (2016).
3. L. Protesescu, S. Yakunin, S. Kumar, J. Bär, F. Bertolotti, N. Masciocchi, A. Guagliardi, M. Grotevent, I. Shorubalko, M.I. Bodnarchuk, C.J. Shih, and M.V. Kovalenko, Dismantling the "Red Wall" of colloidal perovskites: highly luminescent formamidinium and formamidinium-cesium lead iodide nanocrystals. *ACS Nano* 11, 3119 (2017).
4. Q.A. Akkerman, G. Rainò, M.V. Kovalenko, and L. Manna, Genesis, challenges and opportunities for colloidal lead halide perovskite nanocrystals. *Nat. Mater.* 17, 394 (2018).
5. P. Fu, Q. Shan, Y. Shang, J. Song, H. Zeng, Z. Ning, and J. Gong, Perovskite nanocrystals: synthesis, properties and applications. *Sci. Bull.* 62, 369 (2017).
6. X. Gong, M. Li, X. Shi, H. Ma, Z. Wang, and L. Liao, Controllable perovskite crystallization by water additive for high-performance solar cells. *Adv. Funct. Mater.* 25, 6671 (2015).
7. H. Kim, C. Lee, J. Im, K. Lee, T. Moehl, A. Marchioro, S. Moon, R. Humphry-Baker, J. Yum, J.E. Moser, M. Grätzel, and N. Park, Lead iodide perovskite sensitized all-solid-state submicron thin film mesoscopic solar cell with efficiency exceeding 9%. *Sci. Rep.* 2, 591 (2012).
8. X. Li, Y. Wu, S. Zhang, B. Cai, Y. Gu, J. Song, and H. Zeng, CsPbX3 Quantum dots for lighting and displays: room-temperature synthesis, photoluminescence superiorities, underlying origins and white light-emitting diodes. *Adv. Funct. Mater.* 26, 2435 (2016).
9. J. Song, J. Li, X. Li, L. Xu, Y. Dong, and H. Zeng, Quantum dot light-emitting diodes based on inorganic perovskite cesium lead halides ($CsPbX_3$). *Adv. Mater.* 27, 7162 (2015).
10. H. Zhang, Q. Liao, X. Wang, J. Yao, and H. Fu, Water-resistant perovskite polygonal microdisks laser in flexible photonics devices. *Adv. Opt. Mater.* 4, 1718 (2016).
11. Y. Wang, X. Li, J. Song, L. Xiao, H. Zeng, and H. Sun, All-inorganic colloidal perovskite quantum dots: a new class of lasing materials with favorable characteristics. *Adv. Mater.* 27, 7101 (2015).
12. A. Swarnkar, A.R. Marshall, E.M. Sanehira, B.D. Chernomordik, D.T. Moore, J.A. Christians, T. Chakrabarti, and J.M. Luther, Quantum dot-induced phase stabilization of α-$CsPbI_3$ perovskite for high-efficiency photovoltaics. *Science* 354, 92 (2016).
13. L. Persano, A. Camposeo, and D. Pisignano, Advancing the science and technology of electrospinning and functional nanofibers. *Macromol. Mater. Eng.* 302, 1700237 (2017).
14. I. Savva and T. Krasia-Christoforou, Chapter 2: Encroachment of traditional electrospinning, *Electrospinning–basic research to commercialization*. ed. S. Thomas, K. Ghosal, and E. Kny (London: Royal Society of Chemistry, 2018).
15. P. Sagitha, C.R. Reshmi, O. Manaf, S.P. Sundaran, K. Juraij, and A. Sujith, Chapter-8 Development of nanocomposite membranes by electrospun nanofibrous materials, *Nanocomposite membranes for water and gas separation*. ed. M. Sadrzadeh, and T. Mohammadi (Netherlands: Elsevier, 2020).
16. Y. Wang, T. Yokota, and T. Someya, Electrospun nanofiber-based soft electronics. *NPG Asia Mater.* 13, 22 (2021).
17. J. Xue, J. Xie, W. Liu, and Y. Xia, Electrospun nanofibers: new concepts, materials, and applications. *Acc. Chem. Res.* 50, 1976 (2017).
18. J. Xue, T. Wu, Y. Dai, and Y. Xia, Electrospinning and electrospun nanofibers: methods, materials, and applications. *Chem. Rev.* 119, 5298 (2019).
19. C. Zhang and S. Yu, Nanoparticles meet electrospinning: recent advances and future prospects. *Chem. Soc. Rev.* 43, 4423 (2014).
20. J.L. Skinner, J.M. Andriolo, J.P. Murphy, and B.M. Ross, Electrospinning for nano- to mesoscale photonic structures. *Nanophotonics* 6, 765 (2017).
21. Y. Yuan and A. Tang, Progress on the controllable synthesis of all-inorganic halide perovskite nanocrystals and their optoelectronic applications. *J. Semicond.* 41, 011201 (2020).
22. G. Li, Z. Jiang, W. Wang, Z. Chu, Y. Zhang, and C. Wang, Electrospun PAN/$MAPbI_3$ composite fibers for flexible and broadband photodetectors. *Nanomaterials* 9, 50 (2019).
23. D. Chen and Y. Zhu, Electrospun perovskite nanofibers. *Nanoscale Res. Lett.* 12, 114 (2017).
24. H. Zhang, D. Fu, Z. Du, H. Fu, G. Shao, W. Yang, and J. Zheng, In situ growth of aligned $CsPbBr_3$ nanorods in polymer fibers with tailored aspect ratios. *Ceram. Int.* 46, 18352 (2020).
25. H. Liao, S. Guo, S. Cao, L. Wang, F. Gao, Z. Yang, J. Zheng, and W. Yang, A general strategy for in situ growth of all-inorganic $CsPbX_3$ (X = Br, I, and Cl) perovskite nanocrystals in polymer fibers toward significantly enhanced water/thermal stabilities. *Adv. Opt. Mater.* 6, 1800346 (2018).

26. Y. Li, M. Xu, Y. Xia, J. Wu, X. Sun, S. Wang, G. Hu, and C. Xiong, Multilayer assembly of electrospun/electrosprayed PVDF-based nanofibers and beads with enhanced piezoelectricity and high sensitivity. *Chem. Eng. J.* 388, 124205 (2020).
27. P.G. Papagiorgis, A. Manoli, A. Alexiou, P. Karacosta, X. Karagiorgis, G. Papaparaskeva, C. Bernasconi, M.I. Bodnarchuk, M.V. Kovalenko, T. Krasia-Christoforou, and G. Itskos, Robust hydrophobic and hydrophilic polymer fibers sensitized by inorganic and hybrid lead halide perovskite nanocrystal emitters. *Front. Chem.* 7, 87 (2019).
28. M. Grätzel, The light and shade of perovskite solar cells. *Nat. Mater.* 13, 838 (2014).
29. H. Huang, M.I. Bodnarchuk, S.V. Kershaw, M.V. Kovalenko, and A.L. Rogach, Lead halide perovskite nanocrystals in the research spotlight: stability and defect tolerance. *ACS Energy Lett.* 2, 2071 (2017).
30. J. Liu, Z. Yang, B. Ye, Z. Zhao, Y. Ruan, T. Guo, X. Yu, G. Chen, and S. Xu, A review of stability-enhanced luminescent materials: fabrication and optoelectronic applications. *J. Mater. Chem. C* 7, 4934 (2019).
31. D.H. Jiang, Y.H. Tsai, L. Veeramuthu, F.C. Liang, L.C. Chen, C.C. Lin, T. Satoh, S.H. Tung, and C.C. Kuo, Novel ultra-stable and highly luminescent white light-emitting diodes from perovskite quantum dots-polymer nanofibers through biaxial electrospinning. *APL Mater.* 7, 111105 (2019).
32. P.C. Tsai, J.Y. Chen, E. Ercan, C.C. Chueh, S.H. Tung, and W.C. Chen, Uniform luminous perovskite nanofibers with color-tunability and improved stability prepared by one-step core/shell electrospinning. *Small* 14, 1 (2018).
33. C.C. Lin, D.H. Jiang, C.C. Kuo, C.J. Cho, Y.H. Tsai, T. Satoh, and C. Su, Water-resistant efficient stretchable perovskite-embedded fiber membranes for light-emitting diodes. *ACS Appl. Mater. Interfaces* 10, 2210 (2018).
34. K. Ma, X.-Y. Du, Y.-W. Zhang, and S. Chen, In situ fabrication of halide perovskite nanocrystals embedded in polymer composites via microfluidic spinning microreactors. *J. Mater. Chem. C* 5, 9398 (2017).
35. E. Ercan, P.-C. Tsai, J.-Y. Chen, J.-Y. Lam, L.-C. Hsu, C.-C. Chueh, and W.-C. Chen, Stretchable and ambient stable perovskite/polymer luminous hybrid nanofibers of multicolor fiber mats and their white led applications. *ACS Appl. Mater. Interfaces* 11, 23605 (2019).
36. L. Li, Z. Zhang, C. Ding, and J. Xu, Boosting charge separation and photocatalytic CO_2 reduction of $CsPbBr_3$ perovskite quantum dots by hybridizing with P3HT. *Chem. Eng. J.* 419, 129543 (2021).
37. Z. Zhang, L. Liu, H. Huang, L. Li, Y. Wang, J. Xu, and J. Xu, Encapsulation of $CsPbBr_3$ perovskite quantum dots into PPy conducting polymer: exceptional water stability and enhanced charge transport property. *Appl. Surf. Sci.* 526, 146735 (2020).
38. M. Shu, R. Li, and Z. Zhang, $CsPbI_3$ quantum dots/polypyrrole microrod 0D/1D heterostructure: synthesis, formation mechanism and enhanced charge transport property. *Mater. Chem. Phys.* 274, 125193 (2021).
39. Z. Zhang, L. Li, L. Liu, X. Xiao, H. Huang, and J. Xu, Water-stable and photoelectrochemically active $CsPbBr_3$/polyaniline composite by a photocatalytic polymerization process. *J. Phys. Chem. C* 124, 22228 (2020).
40. Q. Hu, E. Rezaee, Q. Dong, H. Shan, Q. Chen, L. Wang, B. Liu, J. Pan, and Z. Xu, P3HT/phthalocyanine nanocomposites as efficient hole-transporting materials for perovskite solar cells. *Sol. RRL* 3, 1800264 (2019).
41. A. Hiltunen, N. Lamminen, H. Salonen, M. Liu, and P. Vivo, Efficiency improvement for perovskite-inspired $Cs_3Sb_2I_9$ solar cells using P3HT as the hole transport material. *Sustain Energy Fuels* 6, 217 (2022).
42. T. Schoetz, M. Ueda, A. Bund, and C. Ponce de Leon, Preparation and characterization of a rechargeable battery based on poly-(3,4-ethylenedioxythiophene) and aluminum in ionic liquids. *J. Solid State Electrochem.* 21, 3237 (2017).
43. T. Jiemsakul, K. Jiramitmongkon, U. Asawapirom, and C. Chotsuwan, Investigation of P3HT electrochromic polymer films prepared by ultrasonication of polymer solutions. *J. Mater. Sci.* 52, 8485 (2017).
44. J.W. Jeong, J.W. Huh, J.I. Lee, H.Y. Chu, J.J. Pak, and B.K. Ju, Interdigitated electrode geometry effects on the performance of organic photoconductors for optical sensor applications. *Thin Solid Films* 518, 6343 (2010).
45. B. Yang, W. Bi, F. Jin, X. Ma, and S. Guo, Surface molecular engineering of $CsPbBr_3$ perovskite nanosheets for high-performance photodetector. *Compos. Commun.* 29, 101032 (2022).
46. U. Lange, N.V. Roznyatovskaya, and V.M. Mirsky, Conducting polymers in chemical sensors and arrays. *Anal. Chim. Acta* 614, 1 (2008).
47. S. Bera, S.B. Singh, and S.K. Ray, Green route synthesis of high quality CdSe quantum dots for applications in light emitting devices. *J. Solid State Chem.* 189, 75 (2012).
48. K. Liu, B. Ouyang, X. Guo, Y. Guo, and Y. Liu, Advances in flexible organic field-effect transistors and their applications for flexible electronics. *npj Flex Electron.* 6, 1 (2022).
49. M. Benhaliliba, A.B. Ahmed, M. Kaleli, and S.E. Meftah, Structural, optical, nonlinear optical HUMO-LUMO properties and electrical characterization of Poly(3-hexylthiophene) (P3HT). *Opt. Mater.* 132, 112782 (2022).
50. T. Blachowicz and A. Ehrmann, Conductive Electrospun Nanofiber Mats. *Materials (Basel)* 13, 152 (2020).
51. A. Laforgue and L. Robitaille, Fabrication of poly-3-hexylthiophene/polyethylene oxide nanofibers using electrospinning. *Synth. Met.* 158, 577 (2008).
52. D. Hernández-Martínez, M.E. Nicho, G. Alvarado-Tenorio, S. García-Carvajal, M. Castillo-Ortega, and C. Vásquez-López, Elaboration and characterization of P3HT–PEO–SWCNT fibers by electrospinning technique. *SN Appl. Sci.* 2, 462 (2020).
53. G. Papaparaskeva, P. Papagiorgis, G. Itskos, and T. Krasia-Christoforou, Highly aligned electrospun polymer fibers produced using a corrugated static collector. *ACS Appl. Polym. Mater.* 4, 586 (2022).
54. K.J. Babu, G. Kaur, L. Biswal, G. De, and H.N. Ghosh, Ultrafast charge delocalization dynamics of ambient stable $CsPbBr_3$ nanocrystals encapsulated in polystyrene. *Fiber. Chem. Eur. J.* 27, 683 (2021).
55. Y. Xue, T. Yang, Y. Zheng, E. Wang, H. Wang, L. Zhu, Z. Du, X. Hou, and K. Chou, The mechanism of a PVDF/$CsPbBr_3$ perovskite composite fiber as a self-polarization piezoelectric nanogenerator with ultra-high output voltage. *J. Mater. Chem. A.* 10, 21893 (2022).
56. K.J. Babu, G. Kaur, A. Shukla, A. Kaur, H. Bhatt, N. Ghorai, G. De, and H.N. Ghosh, In situ $CsPbBr_3$ architecture engineered in electrospun fibers and its ultrafast charge-transfer dynamics. *Mater. Adv.* 3, 6566 (2022).
57. P. Kumar, N. Ganesh, and K.S. Narayan, Electrospun fibers containing emissive hybrid perovskite quantum dots. *ACS Appl. Mater. Interfaces* 11, 24468 (2019).
58. Y. Huang, T. Wang, J. Zheng, F. Li, W. Lan, F. Zheng, and S. Li, Multiwalled carbon nanotubes/$CsPbX_3$@polyacrylonitrile core/shell nanofibers with ultrahigh water, thermal, and ultraviolet stability. *Macromol. Mater. Eng.* 306, 2100200 (2021).
59. H. Papananou, E. Perivolari, K. Chrissopoulou, and S.H. Anastasiadis, Tuning polymer crystallinity via the appropriate selection of inorganic nanoadditives. *Polymer* 157, 111 (2018).

60. C. Kuo, C. Wang, and W. Chen, Poly(3-hexylthiophene)/poly(methyl methacrylate) core-shell electrospun fibers for sensory applications. *Macromol. Symp.* 279, 41 (2009).
61. H. Chen, R. Li, A. Guo, and Y. Xia, Highly fluorescent $CsPbBr_3$/Ti_{O2} core/shell perovskite nanocrystals with excellent stability. *SN Appl. Sci.* 3, 654 (2021).

Authors and Affiliations

Georgia Papaparaskeva[1] · Maria Lydia Ioannides[1] · Chryso Lambride[1] · Eugenia Tanasă[2] · Theodora Krasia-Christoforou[1]

✉ Georgia Papaparaskeva
papaparaskeva.georgia@ucy.ac.cy

✉ Theodora Krasia-Christoforou
krasia@ucy.ac.cy

[1] Department of Mechanical and Manufacturing Engineering, University of Cyprus, Nicosia, Cyprus

[2] Faculty of Applied Chemistry and Material Science, Politehnica University of Bucharest, Bucharest, Romania